CHAPSO-solubilized γ-secretase was incubated with a recombinant APP-C99-Flag substrate for 6 h at 37 °C, and the Aβ40 and Aβ42 levels were measured by ELISA (WAKO Pure Chemical Industries, Osaka, Japan). For the NICD reporter assay, HEK293 cells in a 12-well plate were transiently transfected with NotchΔE (125 ng), HES-Y (125 ng) and 1.25 ng of the control *Renilla* luciferase reporter plasmid pRL-TK (Promega, Osaka, Japan). The cells were lysed 24 h after transfection, and firefly and *Renilla* luciferase activities were quantified using a dual luciferase reporter assay system (Promega) and a luminometer AB-2250 (Atto, Tokyo, Japan). β-Secretase activity of cell lysates was measured using a fluorometric reaction based on β-secretase cleavage of a synthetic substrate (R&D Systems).

Organotypic brain culture. Sagittal forebrain slices containing the hippocampus and cerebral cortex (400-μm thick) were prepared from 3-week-old female Wistar rats using a vibratome (Lancer Vibratome Series 1000, Vibratome, St Louis, MO, USA). The slices were cultured on semi-porous membrane inserts in six-well plates (0.4-μm pore diameter, Millipore) in a 37 °C, 5% CO_2, 99% humidity incubator. The slices were maintained in standard medium consisting of DMEM Ham's F12, 2% B27 neuronal supplement (Invitrogen) and antibiotic mixture (5 μg ml^{-1} penicillin, 5 μg ml^{-1} streptomycin and 10 μg ml^{-1} gentamycin). After 48 h, slices were treated with 10 ng ml^{-1} TGF-β1 (PeproTech, Rocky Hill, CT, USA) and rat ILEI-specific or non-targeting siRNA (Dharmacon) in Accell siRNA Delivery medium (Dharmacon) for another 48 h.

Autopsy human brain tissues. Frozen brain tissues from the frontal and temporal cortices of 15 patients with AD, 15 age-matched non-neurological disease control subjects and 10 non-AD neurological disease control subjects were obtained from the Brain Bank for Aging Research, Tokyo Metropolitan Institute of Gerontology (Tokyo, Japan). All the study subjects or their next of kin gave written informed consent for the brain donation, and the Shiga University of Medical Science Review Board approved the study protocol. All patients with AD fulfilled the National Institute of Neurological and Communicative Disorders and Stroke-Alzheimer's Disease and Related Disorders Associations criteria for probable AD.

Mice. The Tg vector pMoPrP-ILEI was constructed by subcloning an *Xho*I–*Xho*I fragment of human ILEI cDNA into the *Xho*I site of the MoPrP vector that contains the mouse prion promoter to achieve neuron-specific expression[34]. Tg mice were generated by injection of linearized pMoPrP-ILEI DNA into fertilized C57BL/6 mouse oocytes using standard techniques. Tg founders were identified using PCR (see below). Five founders from each injection were backcrossed to C57BL/6 mice for one to two generations before protein and morphology analysis, and the two lines with the highest expression levels were retained for further experiments. The genotypes of Tg mice were determined by PCR using the following transgene-specific primer pair; mPrP-s 5′-CTGCTCCATTTTGC GTGACTC-3′ and hFAM3C-as 5′-CTTCCAGGCAGATTTTGGGTC-3′. APP-Tg (Tg2576) mice[33] were obtained from Taconic Farms (Hudson, NY, USA) and were bred by mating male mice with ILEI-Tg females. Female littermates were used in this study unless otherwise stated. All animal experiments were performed in accordance with national guidelines (Ministry of Education, Culture, Sports, Science, and Technology) and approved by the Shiga University of Medical Science Institutional Animal Care and Use Committees.

Measurement of Aβ in mouse brains. The right halves of mouse brains were homogenized using a motor-driven Teflon/glass homogenizer (ten strokes) in four volumes of Tris-buffered saline (20 mM Tris (pH 7.5), 150 mM NaCl, 0.5 mM EDTA) that contained a protease inhibitor cocktail. The homogenates were centrifuged at 100,000 *g* for 20 min on a TLA 100.4 rotor in a TLX ultracentrifuge (Beckman, Palo Alto, CA, USA). The supernatant was used as the soluble fraction. The pellet was lysed by brief sonication in an initial volume of 6 M guanidine hydrochloride in 50 mM Tris (pH 7.5), and then centrifuged at 100,000 *g* for 10 min. The supernatant was diluted at 1:12 and used as the insoluble fraction. The soluble and insoluble fractions were subjected to a DC protein assay (BioRad) and ELISA assays specific for mouse/rat Aβ40 and Aβ42 (IBL, Gunma, Japan) or for human Aβ40 and Aβ42 (WAKO Pure Chemical Industries). For quantification of Aβ plaque load on brain sections immunostained with anti-human Aβ (1:2,000, IBL), the number of and percentage area occupied by cortical and hippocampal plaques were measured on digital pictures with the ImageJ 1.46 program (National Institutes of Health, Bethesda, MD, USA).

Immunohistochemistry. The left halves of mouse brains were fixed in 4% paraformaldehyde in phosphate buffer. After blocking endogenous peroxidase activity, free-floating brain sections were incubated with appropriately diluted primary antibodies in PBS containing 2% BSA and 0.3% Triton-X100 at 4 °C overnight under horizontal agitation. Sections were then incubated with biotinylated secondary antibodies for 1 h. The immunoreactive products were visualized by incubating with 3,3′-diaminobenzidine containing nickel ammonium sulphate as an enhancing reagent. Stained sections were observed using a microscope (Olympus BX50, Tokyo, Japan). For double fluorescent immunostaining, sections were incubated with a mixture of rabbit polyclonal anti-ILEI antibody (1:4,000) and mouse monoclonal antibody against non-phosphorylated neurofilament (1:4,000, Covance), glial fibrillary acidic protein (1:4,000, Dako, Tokyo, Japan) or Iba1 (1:2,000, WAKO Pure Chemical Industries) overnight at 4 °C, then reacted with a mixture of secondary antibodies conjugated with Alexa488 (1:500, green) and Alexa594 (1:500, red) (Molecular Probes). The stained sections were analysed using a confocal laser-scanning microscope system (Digital Eclipse C1si-Ready, Nikon, Tokyo, Japan).

Y-maze test. The Y-maze apparatus consisted of three arms with grey walls (40 cm long, 10 cm wide, 10 cm high). The insides of the arms were identical, providing no intramaze cues. Each mouse was placed in the centre of the symmetrical Y-maze and was allowed to explore the maze freely for 8 min. The number and sequence of arms entered were recorded manually. The total number of arm entries was used to measure locomotor activity and motivation to explore the maze. The percentage of alternation, which was calculated by the proportion of alternations (an arm choice differing from the previous two choices) to the total number of alternation opportunities (total arm entries minus two), was used as a measure of spatial working memory. Experiments were done blind regarding the genotype of the mice.

Statistical analysis. Statistical evaluation was performed using two-tailed unpaired Student's *t*-test unless otherwise stated. Data are presented as means ± s.d. Statistical significance was defined at $^{*}P<0.05$ or $^{**}P<0.01$.

References

1. De Strooper, B., Iwatsubo, T. & Wolfe, M. S. Presenilins and γ-secretase: structure, function, and role in Alzheimer disease. *Cold Spring Harb. Perspect. Med.* **2,** a006304 (2012).
2. Muller, U. C. & Zheng, H. Physiological functions of APP family proteins. *Cold Spring Harb. Perspect. Med.* **2,** a006288 (2012).
3. Ring, S. *et al.* The secreted β-amyloid precursor protein ectodomain APPsα is sufficient to rescue the anatomical, behavioral, and electrophysiological abnormalities of APP-deficient mice. *J. Neurosci.* **27,** 7817–7826 (2007).
4. St George-Hyslop, P. H. & Petit, A. Molecular biology and genetics of Alzheimer's disease. *C. R. Biol.* **328,** 119–130 (2005).
5. Fukumoto, H., Cheung, B. S., Hyman, B. T. & Irizarry, M. C. β-secretase protein and activity are increased in the neocortex in Alzheimer disease. *Arch. Neurol.* **59,** 1381–1389 (2002).
6. Yang, L. B. *et al.* Elevated β-secretase expression and enzymatic activity detected in sporadic Alzheimer disease. *Nat. Med.* **9,** 3–4 (2003).
7. Riederer, B. M., Leuba, G., Vernay, A. & Riederer, I. M. The role of the ubiquitin proteasome system in Alzheimer's disease. *Exp. Biol. Med. (Maywood)* **236,** 268–276 (2011).
8. Nixon, R. A. & Yang, D. S. Autophagy failure in Alzheimer's disease--locating the primary defect. *Neurobiol. Dis.* **43,** 38–45 (2011).
9. Chang, K. A. & Suh, Y. H. Pathophysiological roles of amyloidogenic carboxy-terminal fragments of the β-amyloid precursor protein in Alzheimer's disease. *J. Pharmacol. Sci.* **97,** 461–471 (2005).
10. Bittner, T. *et al.* γ-secretase inhibition reduces spine density *in vivo* via an amyloid precursor protein-dependent pathway. *J. Neurosci.* **29,** 10405–10409 (2009).
11. Wong, G. T. *et al.* Chronic treatment with the γ-secretase inhibitor LY-411,575 inhibits β-amyloid peptide production and alters lymphopoiesis and intestinal cell differentiation. *J. Biol. Chem.* **279,** 12876–12882 (2004).
12. Mitani, Y. *et al.* Differential effects between γ-secretase inhibitors and modulators on cognitive function in amyloid precursor protein-transgenic and nontransgenic mice. *J. Neurosci.* **32,** 2037–2050 (2012).
13. Doody, R. S. *et al.* A phase 3 trial of semagacestat for treatment of Alzheimer's disease. *N. Engl. J. Med.* **369,** 341–350 (2013).
14. De Strooper, B. & Annaert, W. Novel research horizons for presenilins and γ-secretases in cell biology and disease. *Annu. Rev. Cell. Dev. Biol.* **26,** 235–260 (2010).
15. Mitsuishi, Y. *et al.* Human CRB2 inhibits γ-secretase cleavage of amyloid precursor protein by binding to the presenilin complex. *J. Biol. Chem.* **285,** 14920–14931 (2010).
16. Hasegawa, H., Liu, L. & Nishimura, M. Dilysine retrieval signal-containing p24 proteins collaborate in inhibiting γ-cleavage of amyloid precursor protein. *J. Neurochem.* **115,** 771–781 (2010).
17. He, G. *et al.* γ-secretase activating protein is a therapeutic target for Alzheimer's disease. *Nature* **467,** 95–98 (2010).
18. Chen, F. *et al.* TMP21 is a presenilin complex component that modulates γ-secretase but not ε-secretase activity. *Nature* **440,** 1208–1212 (2006).
19. Wakabayashi, T. *et al.* Analysis of the γ-secretase interactome and validation of its association with tetraspanin-enriched microdomains. *Nat. Cell. Biol.* **11,** 1340–1346 (2009).

20. Rigaut, G. *et al.* A generic protein purification method for protein complex characterization and proteome exploration. *Nat. Biotechnol.* **17,** 1030–1032 (1999).
21. Esler, W. P. *et al.* Activity-dependent isolation of the presenilin-γ-secretase complex reveals nicastrin and a γ substrate. *Proc. Natl Acad. Sci. USA* **99,** 2720–2725 (2002).
22. Zhu, Y. *et al.* Cloning, expression, and initial characterization of a novel cytokine-like gene family. *Genomics* **80,** 144–150 (2002).
23. Zhao, G., Liu, Z., Ilagan, M. X. & Kopan, R. γ-secretase composed of PS1/Pen2/Aph1a can cleave Notch and amyloid precursor protein in the absence of nicastrin. *J. Neurosci.* **30,** 1648–1656 (2010).
24. Hasegawa, H. *et al.* Both the sequence and length of the C terminus of PEN-2 are critical for intermolecular interactions and function of presenilin complexes. *J. Biol. Chem.* **279,** 46455–46463 (2004).
25. Pitsi, D. & Octave, J. N. Presenilin 1 stabilizes the C-terminal fragment of the amyloid precursor protein independently of γ-secretase activity. *J. Biol. Chem.* **279,** 25333–25338 (2004).
26. Watanabe, N. *et al.* Functional analysis of the transmembrane domains of presenilin 1: participation of transmembrane domains 2 and 6 in the formation of initial substrate-binding site of γ-secretase. *J. Biol. Chem.* **285,** 19738–19746 (2010).
27. Herreman, A. *et al.* Total inactivation of γ-secretase activity in presenilin-deficient embryonic stem cells. *Nat. Cell Biol.* **2,** 461–462 (2000).
28. Waerner, T. *et al.* ILEI: a cytokine essential for EMT, tumor formation, and late events in metastasis in epithelial cells. *Cancer Cell* **10,** 227–239 (2006).
29. Xia, W. *et al.* Presenilin complexes with the C-terminal fragments of amyloid precursor protein at the sites of amyloid β-protein generation. *Proc. Natl Acad. Sci. USA* **97,** 9299–9304 (2000).
30. Choy, R. W., Cheng, Z. & Schekman, R. Amyloid precursor protein (APP) traffics from the cell surface via endosomes for amyloid β (Aβ) production in the trans-Golgi network. *Proc. Natl Acad. Sci. USA* **109,** E2077–E2082 (2012).
31. Tesseur, I. *et al.* Deficiency in neuronal TGF-β signaling promotes neurodegeneration and Alzheimer's pathology. *J. Clin. Invest.* **116,** 3060–3069 (2006).
32. Chaudhury, A. *et al.* TGF-β-mediated phosphorylation of hnRNP E1 induces EMT via transcript-selective translational induction of Dab2 and ILEI. *Nat. Cell Biol.* **12,** 286–293 (2010).
33. Hsiao, K. *et al.* Correlative memory deficits, Aβ elevation, and amyloid plaques in transgenic mice. *Science* **274,** 99–102 (1996).
34. Borchelt, D. R. *et al.* A vector for expressing foreign genes in the brains and hearts of transgenic mice. *Genet. Anal.* **13,** 159–163 (1996).
35. Johansson, P. *et al.* FAM3B PANDER and FAM3C ILEI represent a distinct class of signaling molecules with a non-cytokine-like fold. *Structure* **21,** 306–313 (2013).
36. Lahsnig, C. *et al.* ILEI requires oncogenic Ras for the epithelial to mesenchymal transition of hepatocytes and liver carcinoma progression. *Oncogene* **28,** 638–650 (2009).
37. Wilson, C. G., Robert-Cooperman, C. E. & Burkhardt, B. R. PANcreatic-DERived factor: novel hormone PANDERing to glucose regulation. *FEBS Lett.* **585,** 2137–2143 (2011).
38. Katahira, T., Nakagiri, S., Terada, K. & Furukawa, T. Secreted factor FAM3C (ILEI) is involved in retinal laminar formation. *Biochem. Biophys. Res. Commun.* **392,** 301–306 (2010).
39. Caraci, F. *et al.* TGF-β1 pathway as a new target for neuroprotection in Alzheimer's disease. *CNS Neurosci. Ther.* **17,** 237–249 (2011).
40. Caraci, F. *et al.* The CC genotype of transforming growth factor-β1 increases the risk of late-onset Alzheimer's disease and is associated with AD-related depression. *Eur. Neuropsychopharmacol.* **22,** 281–289 (2012).
41. Xiao, F. *et al.* Proteomic analysis of cerebrospinal fluid from patients with idiopathic temporal lobe epilepsy. *Brain Res.* **1255,** 180–189 (2009).
42. Mackenzie, I. R. & Miller, L. A. Senile plaques in temporal lobe epilepsy. *Acta. Neuropathol.* **87,** 504–510 (1994).
43. Davies, H., Blennow, K., McGuire, J., Podust, V. & Simonsen, A. Saponin D and FAM3C are biomarkers for Alzheimer's disease. US Patent 7993868 (2011).
44. Nunan, J. *et al.* The C-terminal fragment of the Alzheimer's disease amyloid protein precursor is degraded by a proteasome-dependent mechanism distinct from γ-secretase. *Eur. J. Biochem.* **268,** 5329–5336 (2001).
45. Flood, F. *et al.* Proteasome-mediated effects on amyloid precursor protein processing at the γ-secretase site. *Biochem. J.* **385,** 545–550 (2005).
46. Caporaso, G. L., Gandy, S. E., Buxbaum, J. D. & Greengard, P. Chloroquine inhibits intracellular degradation but not secretion of Alzheimer β/A4 amyloid precursor protein. *Proc. Natl Acad. Sci. USA* **89,** 2252–2256 (1992).
47. Jaeger, P. A. *et al.* Regulation of amyloid precursor protein processing by the Beclin 1 complex. *PLoS ONE* **5,** e11102 (2010).
48. Lai, M. T. *et al.* Presenilin-1 and presenilin-2 exhibit distinct yet overlapping γ-secretase activities. *J. Biol. Chem.* **278,** 22475–22481 (2003).
49. Sato, C., Takagi, S., Tomita, T. & Iwatsubo, T. The C-terminal PAL motif and transmembrane domain 9 of presenilin 1 are involved in the formation of the catalytic pore of the γ-secretase. *J. Neurosci.* **28,** 6264–6271 (2008).
50. Suzuki, T. & Nakaya, T. Regulation of amyloid β-protein precursor by phosphorylation and protein interactions. *J. Biol. Chem.* **283,** 29633–29637 (2008).
51. Chen, Q., Kimura, H. & Schubert, D. A novel mechanism for the regulation of amyloid precursor protein metabolism. *J. Cell Biol.* **158,** 79–89 (2002).
52. Kashiwa, A. *et al.* Isolation and characterization of novel presenilin binding protein. *J. Neurochem.* **75,** 109–116 (2000).
53. Page, R. M. *et al.* Loss of PAFAH1B2 reduces amyloid-β generation by promoting the degradation of amyloid precursor protein C-terminal fragments. *J. Neurosci.* **32,** 18204–18214 (2012).
54. Tamboli, I. Y. *et al.* Sphingolipid storage affects autophagic metabolism of the amyloid precursor protein and promotes Aβ generation. *J. Neurosci.* **31,** 1837–1849 (2011).
55. Chavez-Gutierrez, L. *et al.* The mechanism of γ-secretase dysfunction in familial Alzheimer disease. *EMBO J.* **31,** 2261–2274 (2012).
56. Nishimura, M. *et al.* Presenilin mutations associated with Alzheimer disease cause defective intracellular trafficking of β-catenin, a component of the presenilin protein complex. *Nat. Med.* **5,** 164–169 (1999).
57. Schroeter, E. H., Kisslinger, J. A. & Kopan, R. Notch-1 signalling requires ligand-induced proteolytic release of intracellular domain. *Nature* **393,** 382–386 (1998).
58. Tagami, S. *et al.* Regulation of Notch signaling by dynamic changes in the precision of S3 cleavage of Notch-1. *Mol. Cell Biol.* **28,** 165–176 (2008).
59. Iijima, M. *et al.* Nanocapsules incorporating IgG Fc-binding domain derived from *Staphylococcus aureus* protein A for displaying IgGs on immunosensor chips. *Biomaterials* **32,** 1455–1464 (2011).
60. Edbauer, D., Willem, M., Lammich, S., Steiner, H. & Haass, C. Insulin-degrading enzyme rapidly removes the β-amyloid precursor protein intracellular domain (AICD). *J. Biol. Chem.* **277,** 13389–13393 (2002).

Acknowledgements

This work was supported in part by Grants-in-Aid for Scientific Research from the Ministry of Education, Culture, Sports, Science, and Technology, Japan (23500445 to M.N. and 23590359 to H.H.), a grant from the A-STEP, Japan Science and Technology Agency (AS231Z00919G to M.N.) and a grant from the Program for the Promotion of Fundamental Studies in Health Sciences of the National Institute of Biomedical Innovation, Japan (05-26 to M.N.).

Author contributions

H.H. and L.L. performed the TAP and cell culture experiments. L.L. contributed to the organotypic culture and immunohistochemistry experiments. L.L., I.T. and M.N. carried out the Tg mouse experiments. S.M. collected autopsy brain samples and performed neuropathological diagnosis. M.N. designed the study, supervised all of the experiments and wrote the manuscript.

Additional information

Supplementary Information accompanies this paper at http://www.nature.com/naturecommunications

Competing financial interests: The authors declare no competing financial interests.

Reprints and permission information is available online at http://npg.nature.com/reprintsandpermissions/

How to cite this article: Hasegawa, H. *et al.* The FAM3 superfamily member ILEI ameliorates Alzheimer's disease-like pathology by destabilizing the penultimate amyloid-β precursor. *Nat. Commun.* 5:3917 doi: 10.1038/ncomms4917 (2014).

Supplementary Figure 1

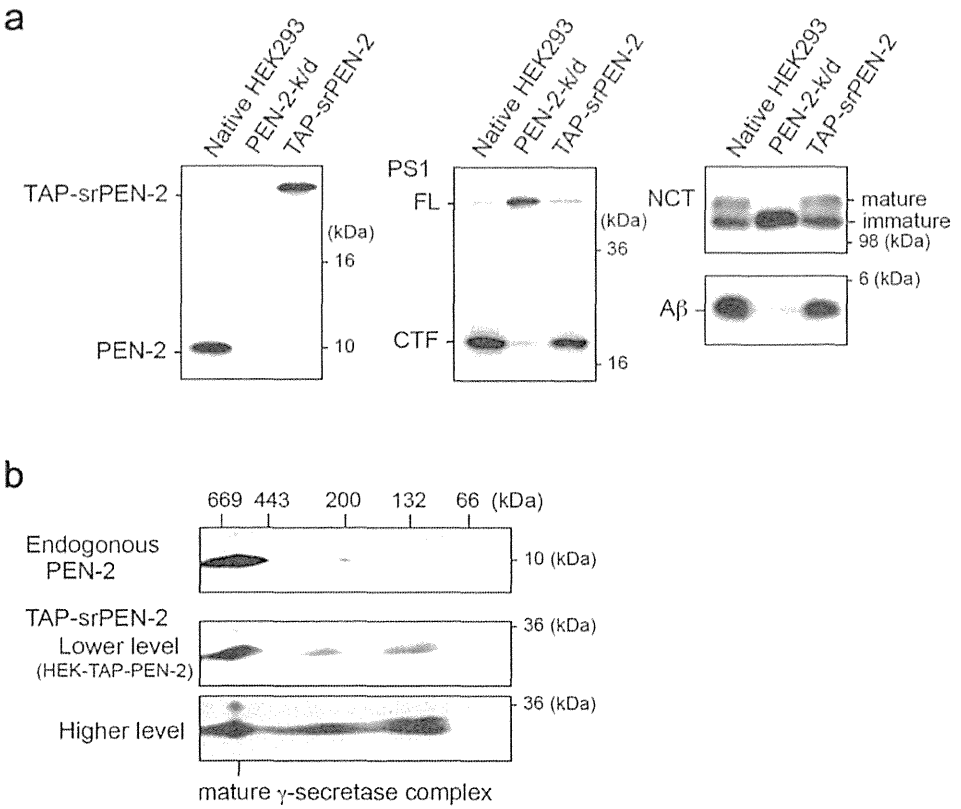

Supplementary Figure 1. Characterization of HEK/TAP-PEN-2 cells

(a) Stable transfection of PEN2-knockdown (k/d) HEK293 cells with TAP-srPEN-2 (left panel) restored proteolysis of PS1 (center panel), glycosylation of NCT (right upper panel), and generation of Aβ (right lower panel). Aβ was immunoprecipitated from the conditioned medium of each cell line and subjected to immunoblotting. **(b)** 2D-BN/SDS-PAGE followed by immunoblotting showed that endogenous PEN-2 was incorporated into the mature γ-secretase complex in native HEK293 cells (upper panel). Most of the transfected TAP-srPEN-2 was incorporated into the mature γ-secretase complex in the HEK-TAP-PEN-2 cell line (middle panel), although a cell line with higher TAP-srPEN-2 expression formed multiple smaller complexes (lower panel). Original immunoblots for (**a**) and (**b**) can be found in Supplementary Fig. 10.

Supplementary Figure 2

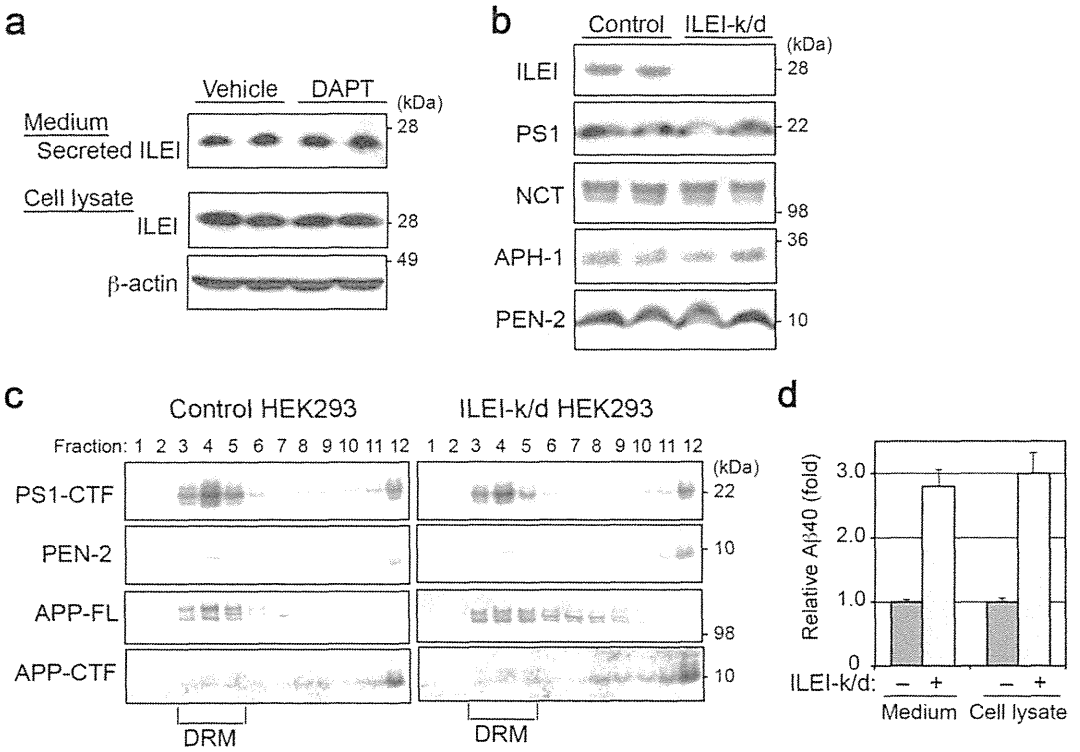

Supplementary Figure 2. ILEI is not a substrate for γ-secretase and does not affect the expression level or the subcellular localization of the γ-secretase complex, or the Aβ secretion process.

(a) DAPT treatment of HEK293 cells did not alter the levels of cellular and secreted ILEI as assessed with immunoblotting. β-actin was used as a loading control. **(b)** ILEI-knockdown (k/d) did not change the expression levels of the indicated γ-secretase components as assessed with immunoblotting. **(c)** ILEI did not detectably affect localization of the γ-secretase complex or APP in detergent-resistant membrane microdomains (DRM). HEK293 cells treated with control or ILEI-specific siRNA were homogenized in MBS buffer (25 mM MES, 150 mM NaCl, pH 6.5) containing 1% Lubrol WX (Lubrol 17A17; Serva) and a protease inhibitor cocktail. The homogenate was centrifuged at 2,000 *g* for 10 min, and the supernatant was adjusted to 40% sucrose in MBS. The sample was transferred to 13-ml ultracentrifuge tubes and overlaid with a 5/10/20/30% discontinuous sucrose gradient in MBS. After centrifugation at 260,000 *g* for 21 h in an SW-41Ti rotor (Beckman Coulter), 1-ml fractions were collected from the top and analyzed with immunoblotting. **(d)** ILEI did not perturb the process of Aβ secretion. ILEI-knockdown increased Aβ levels in both the culture medium and cell lysates of Swedish mutant APP-overexpressing HEK293 cells. Aβ40 concentrations were as follows: control medium, 9.49 ± 0.32 pmol ml^{-1}, ILEI-k/d medium, 26.78 ± 2.86 pmol ml^{-1}; control cell lysate, 13.82 ± 0.88 pmol per g protein; ILEI-k/d cell lysate, 42.55 ± 5.82 pmol per g protein ($n = 3$, mean ± s.d.). $P > 0.05$ by Student's *t*-test. Original immunoblots for (**a-c**) can be found in Supplementary Fig. 10.

Supplementary Figure 3

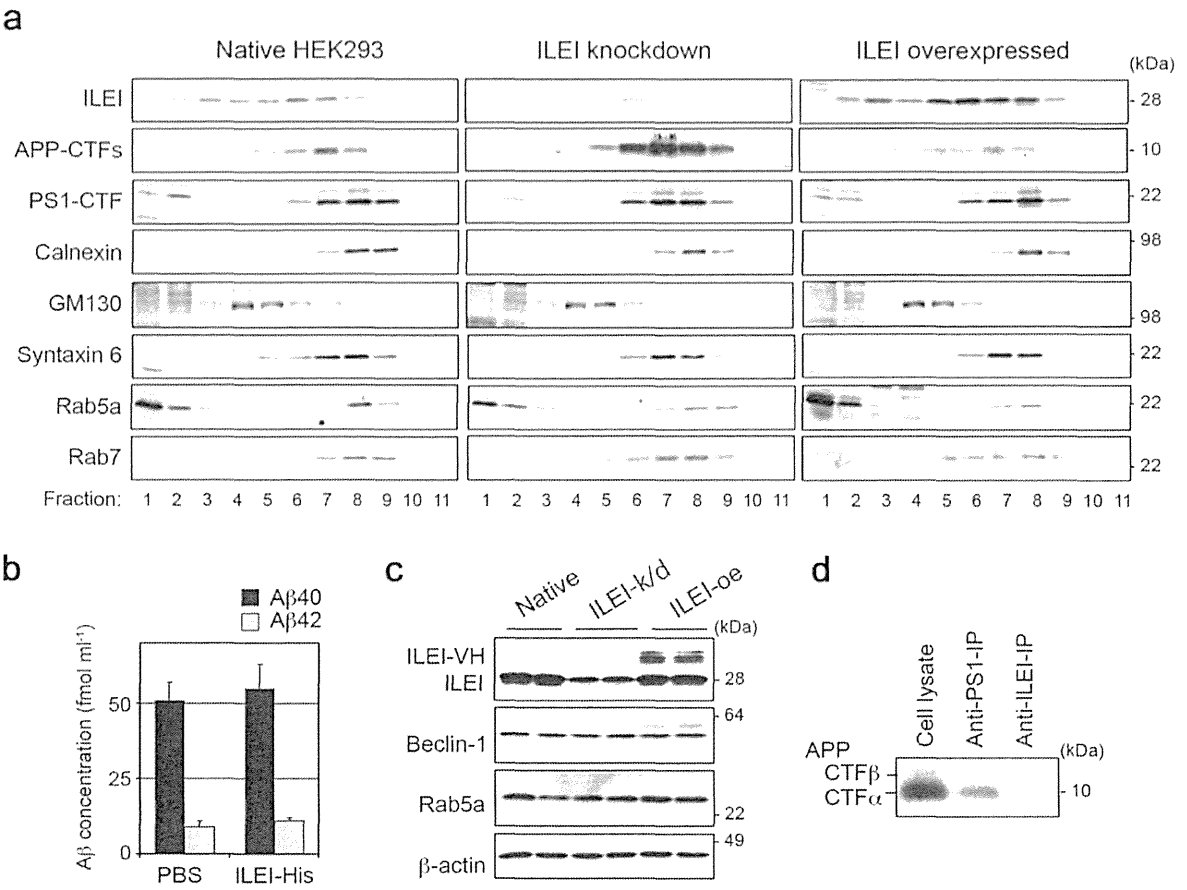

Supplementary Figure 3. ILEI does not alter the general activity of autophagy, lysosomal protein degradation, or subcellular localization of APP-CTFs.

(a) Subcellular localization of ILEI, APP-CTFs, and PS1-CTF in native, ILEI-knockdown and ILEI-overexpressed HEK293 cells. Membrane fractions were isolated from HEK293 cells and applied onto a discontinuous gradient consisting of 1 ml each of 30%, 25%, 20%, 15%, 12.5%, 10%, 7.5%, 5% and 2.5% (v/v) iodixanol. After centrifugation at 126,000 *g* for 1 h, eleven 1.0-ml fractions were collected from the top to the bottom of the gradient and were subjected to immunoblotting with the indicated antibodies. Antibodies against calnexin (1:10,000), GM130 (1:10,000), syntaxin 6 (1:5,000) (BD Transduction Laboratories), Rab5a (1:1,000), and Rab7 (1:500) (Santa Cruz Biotechnology) were used as markers of the endoplasmic reticulum, *cis*-Golgi, *trans*-Golgi, early endosomes, and late endosomes, respectively. **(b)** ILEI did not enhance Aβ degradation in the culture medium. The conditioned medium of ILEI-knockdown cells was incubated with PBS or purified ILEI-VH (5 μg ml^{-1}) at 37 °C for 6 h. Aβ levels were measured using ELISAs ($n = 3$, mean ± s.d.). $P > 0.05$ by Student's *t*-test. **(c)** Lysates of native, ILEI-knockdown (k/d), and ILEI-overexpressing (oe) HEK293 cells were subjected to immunoblotting for ILEI, Beclin-1, and Rab5a. β-actin was used as a loading control. **(d)** Co-immunoprecipitation of ILEI and APP-CTFs. Native HEK293 cell lysates were immunoprecipitated with normal IgG or an antibody against ILEI. The blot was probed with anti-APP-CTF antibody. Anti-PS1 precipitate served as a positive control. Original immunoblots for **(a)**, **(c)** and **(d)** can be found in Supplementary Fig. 10.

Supplementary Figure 4

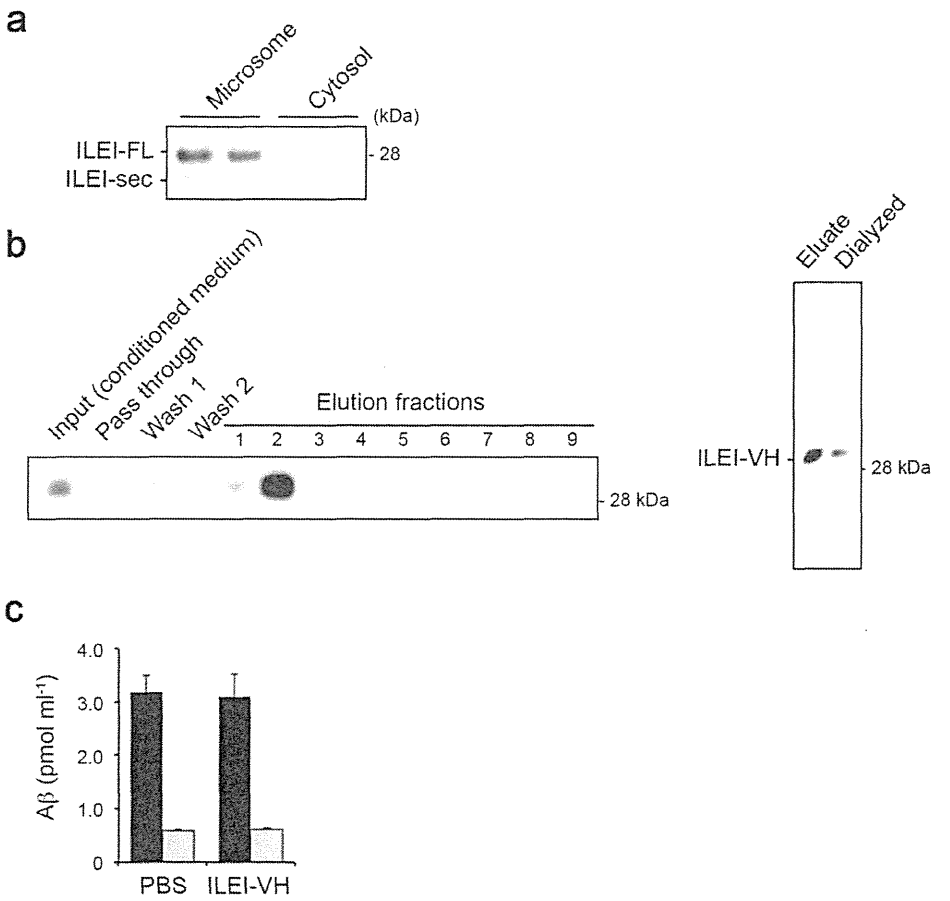

Supplementary Figure 4. Purification of secreted ILEI-VH peptide

(a) Intracellular ILEI was mostly associated with the microsome fraction. The homogenate of HEK293 cells was centrifuged at 1,000 *g*, and the supernatant was further ultracentrifuged at 100,000 *g* for 1 h to yield crude microsome (pellet) and cytosol (supernatant) fractions, which were then assayed with immunoblotting for ILEI. **(b)** Purification of the ILEI-VH peptide. The conditioned medium of HEK293 cells stably overexpressing C-terminally V5-6xHis-tagged ILEI (ILEI-VH) was cleared with brief centrifugation and then incubated with Ni-nitrilotriacetic acid-agarose (Qiagen) for 8 h at 4 °C. After washing twice with PBS, the secreted ILEI-VH was eluted with 200 mM imidazole. The fractions were assayed with immunoblotting for ILEI (left panel). The eluted fraction #2 was dialyzed against PBS. The purity of the ILEI-VH fractions was tested using SDS-PAGE followed by Coomassie Brilliant Blue staining (right panel). **(c)** Purified ILEI-VH did not affect Aβ generation in a cell-free γ-secretase assay. Solubilized γ-secretase complexes prepared from ILEI-knockdown HEK293 cells were incubated with recombinant APP-CTFβ-Flag in the presence or absence of purified ILEI-VH (5 μg ml^{-1}). Aβ40 (black bars) and Aβ42 (grey bars) were measured using ELISAs ($n = 3$, mean ± s.d.). $P > 0.05$ by Student's *t*-test. Original immunoblots for (**a**) and (**b**) can be found in Supplementary Fig. 10.

Supplementary Figure 5

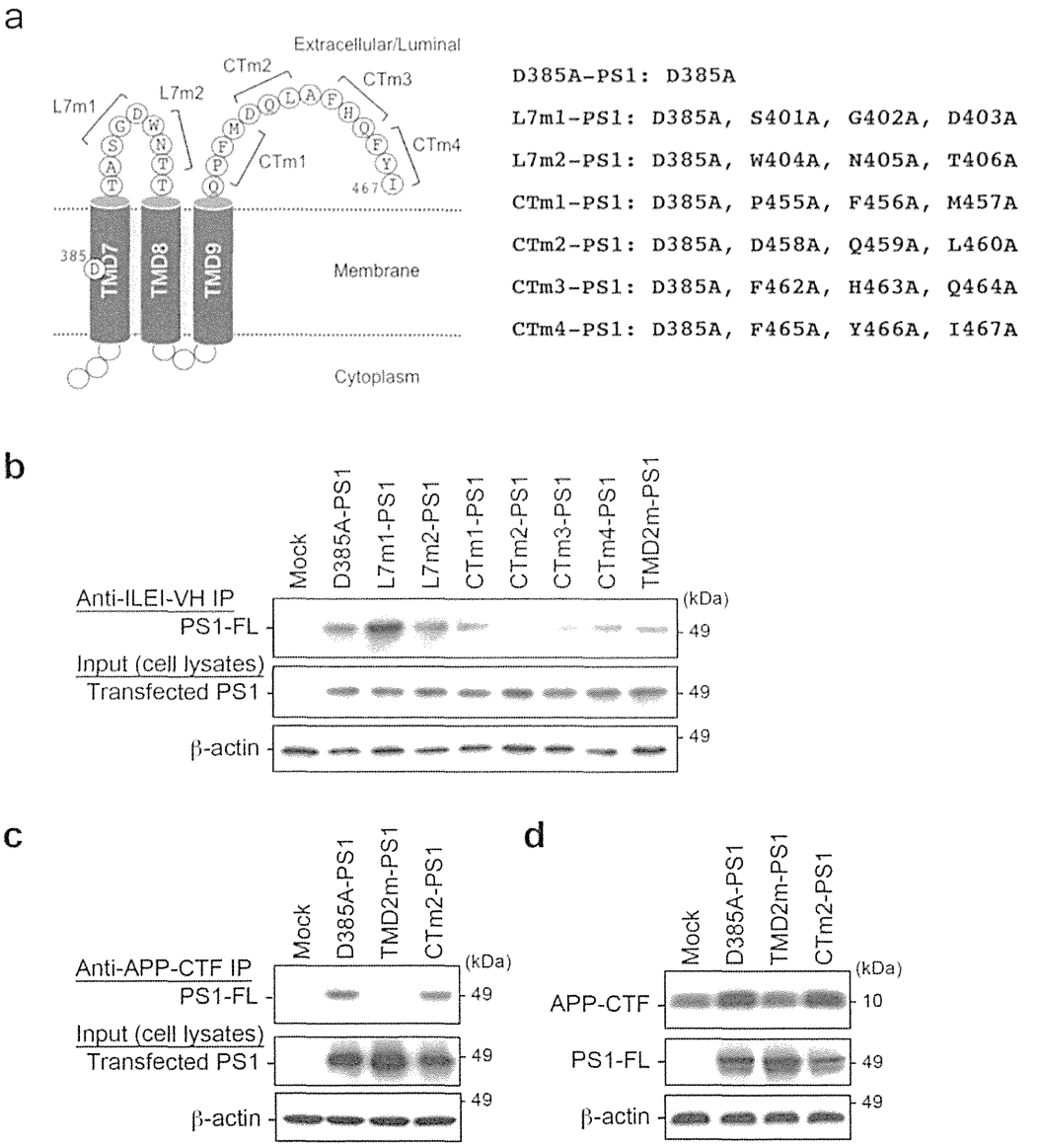

Supplementary Figure 5. Characterization of PS1 mutants

(a) Schematic of PS1 mutants harboring alanine substitutions of the active site aspartate (D^{385}) and three sequential amino acid residues in the extracellular/luminal C-terminal regions. **(b)** Co-immunoprecipitation of mutant PS1 and ILEI. Each PS1 mutant was transiently transfected into HEK293 cells stably expressing ILEI-VH, and IELI-VH was precipitated with anti-V5 antibody. CTm2-PS1 was not co-immunoprecipitated with IELI-VH. **(c)** Co-immunoprecipitation of mutant PS1 and APP. HEK293 cells were transfected with mock, D385A-PS1, TMD2m-PS1, or CTm2-PS1, and then treated with DAPT for 12 h. Anti-APP-CTF precipitates did not contain TMD2m-PS1. **(d)** Mock, D385A-PS1, TMD2m-PS1, or CTm2-PS1 was transfected into PS1/PS2-knockout MEFs. Cell lysates were subjected to immunoblotting for APP-CTFs or PS1. β-actin was used as a loading control. Original immunoblots for **(b-d)** can be found in Supplementary Fig. 10.

Supplementary Figure 6

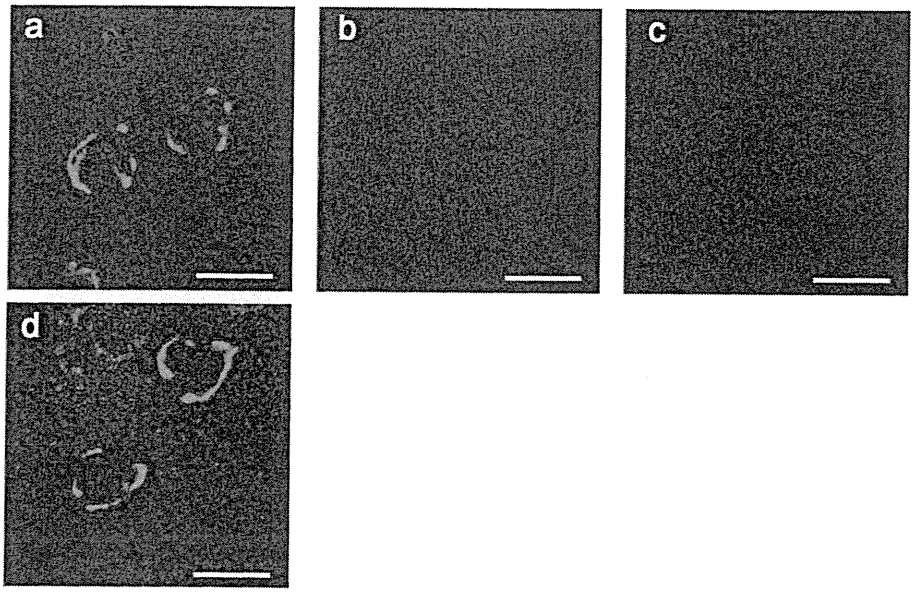

Supplementary Figure 6. Characterization of rabbit polyclonal anti-ILEI antibody

(a) Rabbit polyclonal antibody against a synthetic polypeptide representing the N-terminal sequence of human ILEI immunostained perinuclear vesicular structures in neurons of mouse brain. Incubation with the secondary antibody alone **(b)** or preabsorption of the rabbit antibody with the antigen peptide **(c)** abolished immunostaining. **(d)** Goat polyclonal antibody against human full-length ILEI immunostained similar structures as seen in (a). Scale bars: 10 μm.

Supplementary Figure 7

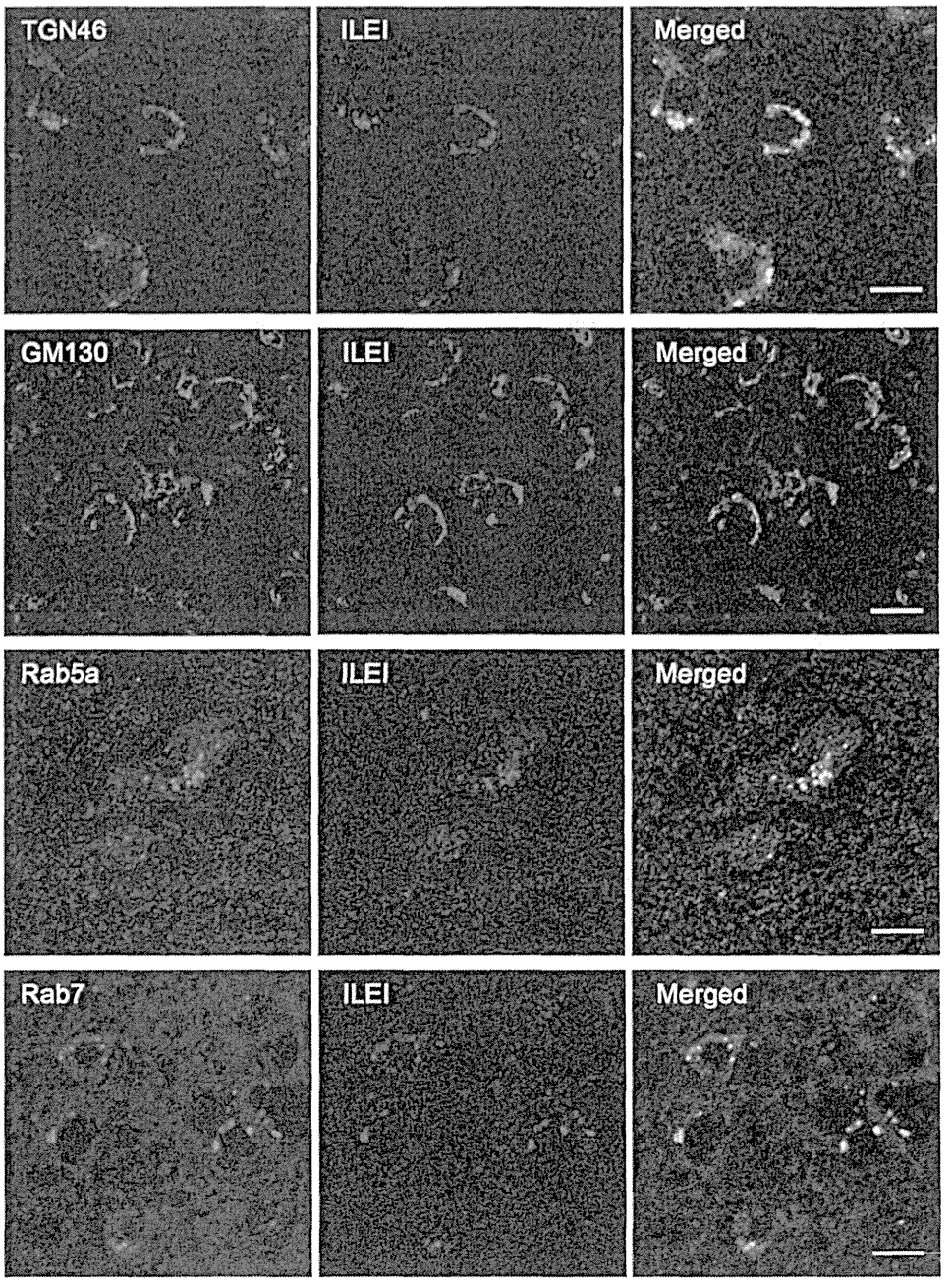

Supplementary Figure 7. ILEI is localized in the *trans*-Golgi network (TGN) and endosomes

Double immunostaining of mouse brain for ILEI and markers of the Golgi complex and endosome compartments. Antibodies against TGN46 (1:4,000, Sigma), GM130 (1:2,000, BD Transduction Laboratories), Rab5a (1:500), and Rab7 (1:300) (Santa Cruz Biotechnology) were used as markers of the TGN, *cis*-Golgi, early endosomes, and late endosomes, respectively. Scale bars: 20 μm.

Supplementary Figure 8

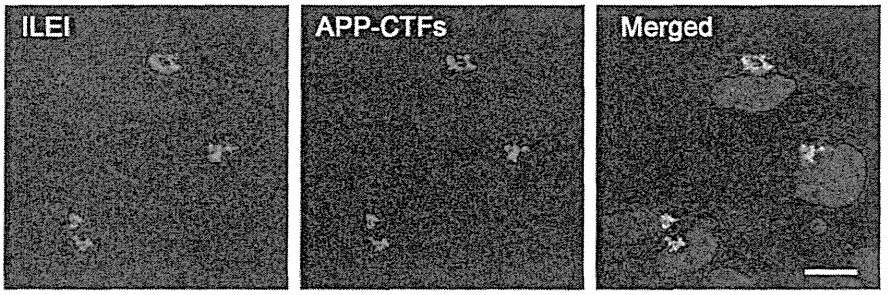

Supplementary Figure 8. Colocalization of ILEI and APP-CTFs

Double immunostaining for ILEI and APP-CTFs. HEK293 cells were stained with anti-ILEI antibody (1:4,000) and anti-APP-CTF antibody (1:3,000, Sigma). Nuclei were stained with Hoechst 33342. Scale bar: 10 μm.

Supplementary Figure 9

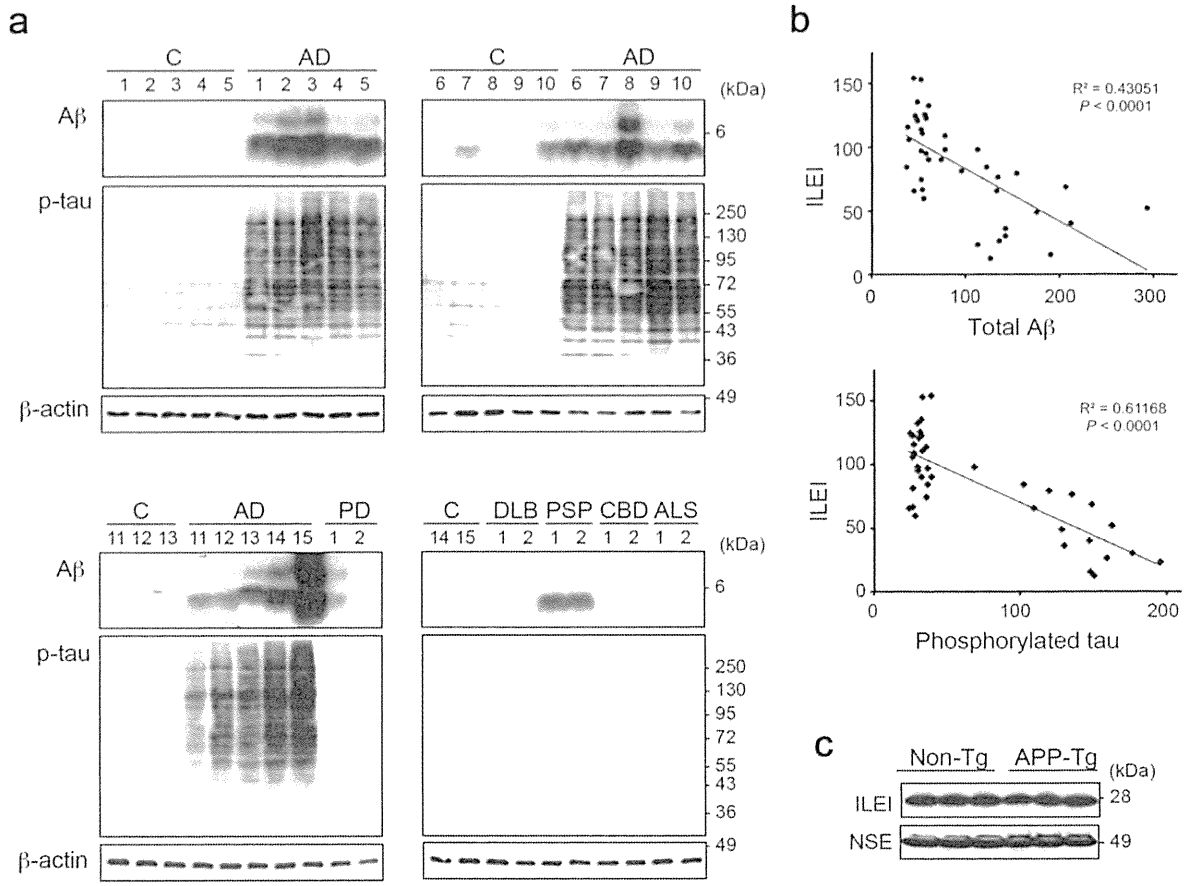

Supplementary Figure 9. Phosphorylated tau, Aβ, and ILEI in autopsy brains and ILEI level in APP-Tg mouse brains

(a) Lysates of temporal cortices of autopsy cases were subjected to immunoblotting for total Aβ and phosphorylated tau (p-tau). Blots were probed with anti-Aβ antibody (1:1,000, 4G8 from Covance) or anti-phosphorylated tau antibody (1:3,000, PHF13 from Millipore). β-actin was used as a loading control. C: control, AD: Alzheimer's disease, PD: Parkinson's disease, DLB: dementia with Lewy bodies, PSP: progressive supranuclear palsy, CBD: corticobasal degeneration, ALS: amyotrophic lateral sclerosis. **(b)** The graphs show the correlation between ILEI (see Fig. 5c) and Aβ or phosphorylated tau. The intensities of total Aβ and phosphorylated tau were measured with Image-J software and normalized to the intensity of β-actin. Linear regressions were performed using a Prism 3.0 software (GraphPad, San Diego, CA, USA). **(c)** Brain lysates from APP-Tg and non-Tg littermate mice (12 months old, $n = 3$ per genotype) were subjected to immunoblotting for ILEI. NSE was used as a loading control. Original immunoblots for (**a**) and (**c**) can be found in Supplementary Fig. 10.

Supplementary Figure 10

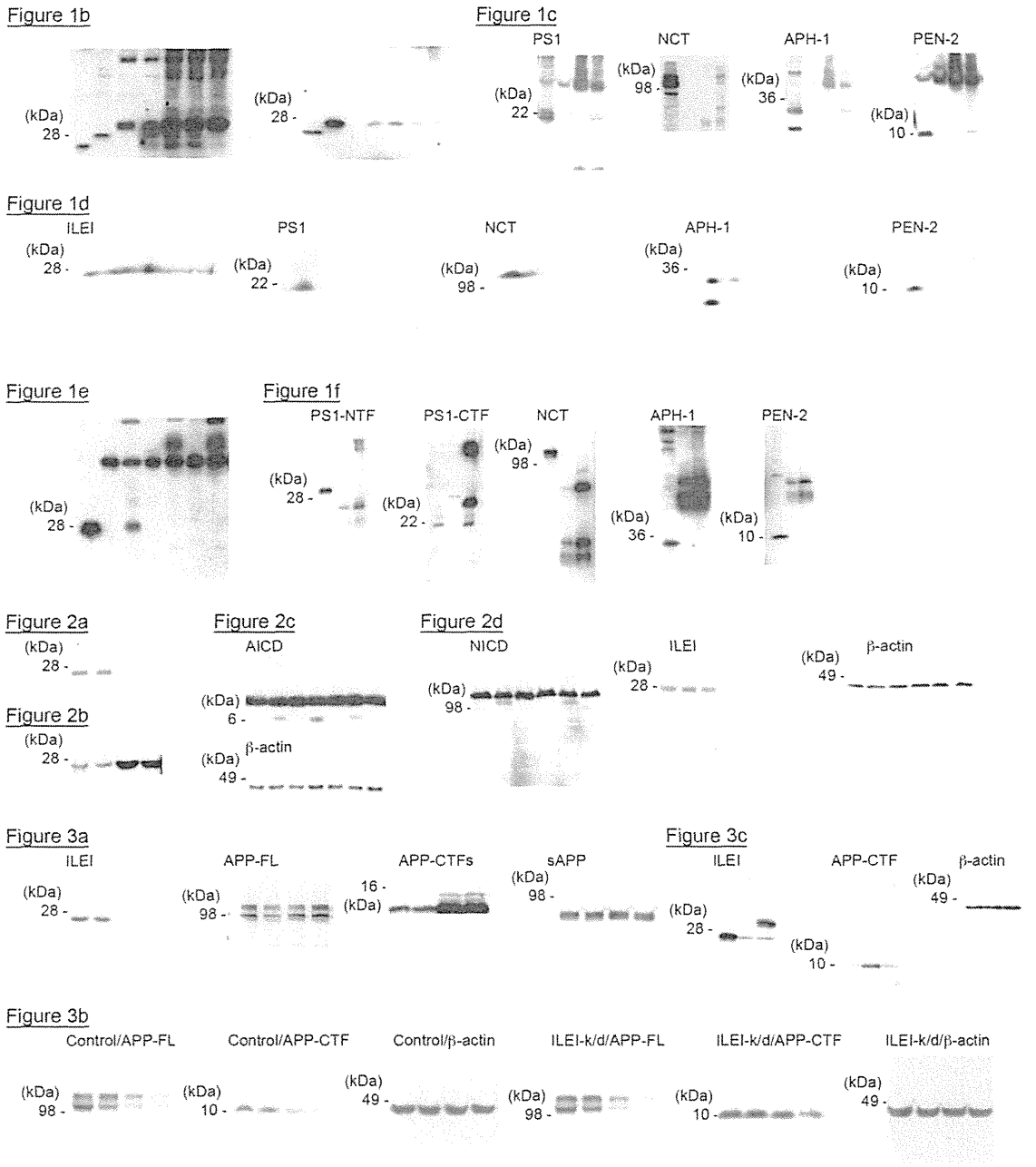

Supplementary Figure 10. Original immunoblots in main and supplementary figures.

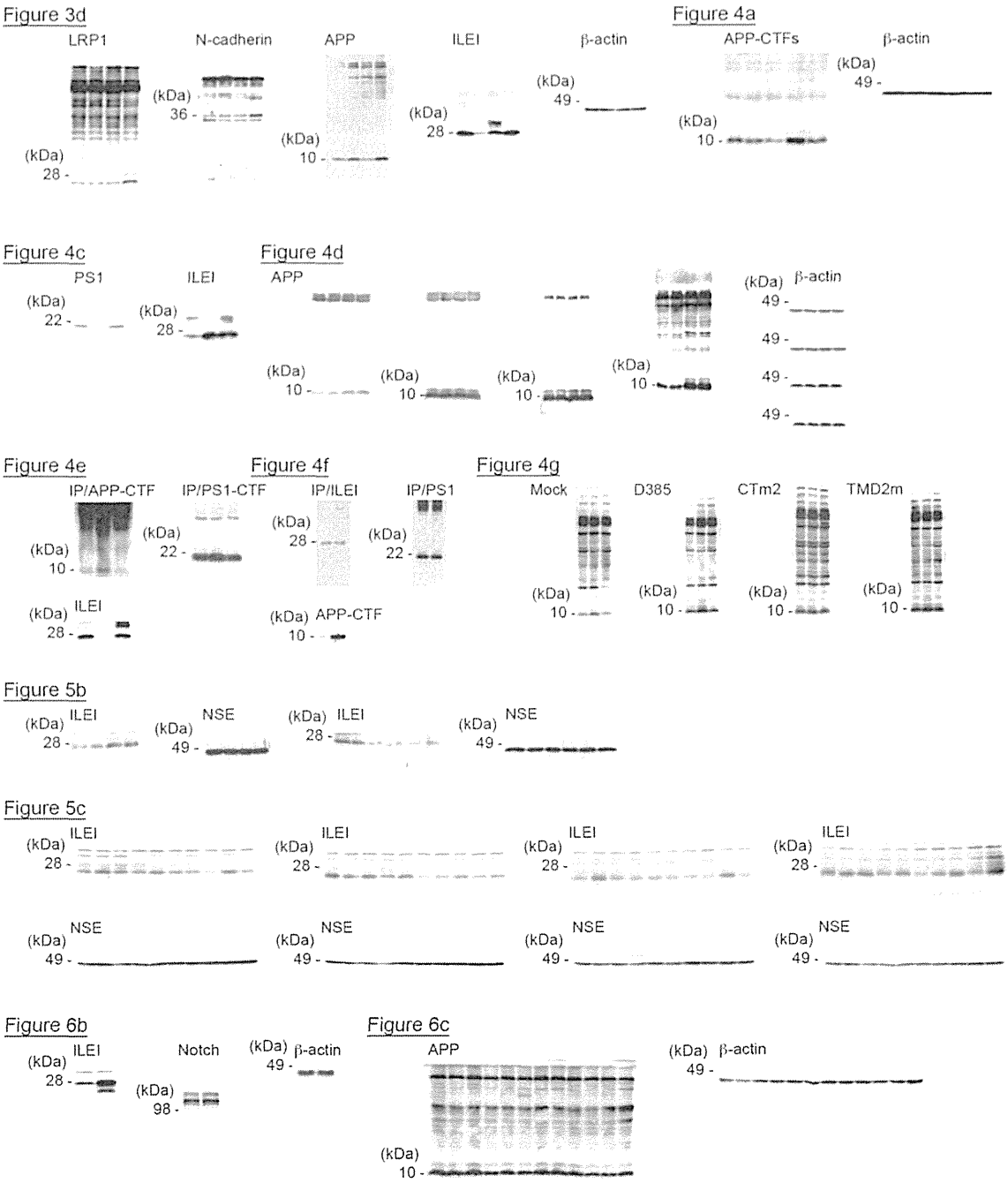

Supplementary Figure 10 continued.

Supplementary Figure 1a

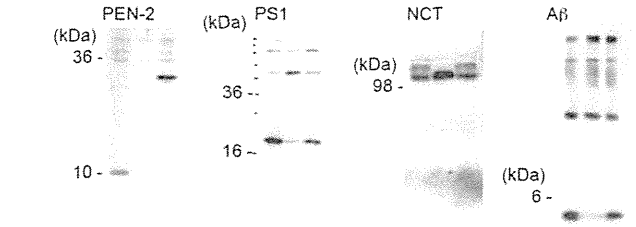

Supplementary Figure 1b

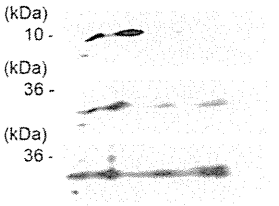

Supplementary Figure 2a

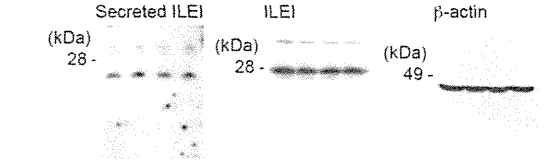

Supplementary Figure 2b

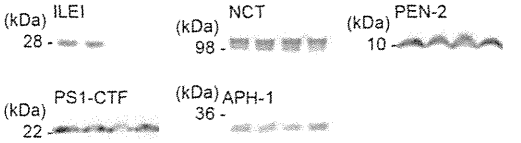

Supplementary Figure 2c

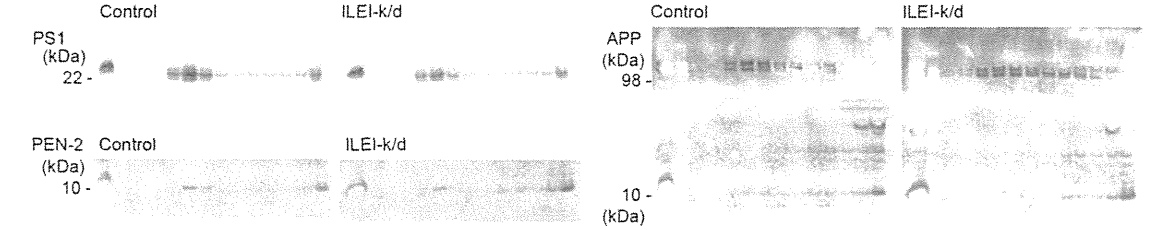

Supplementary Figure 3a

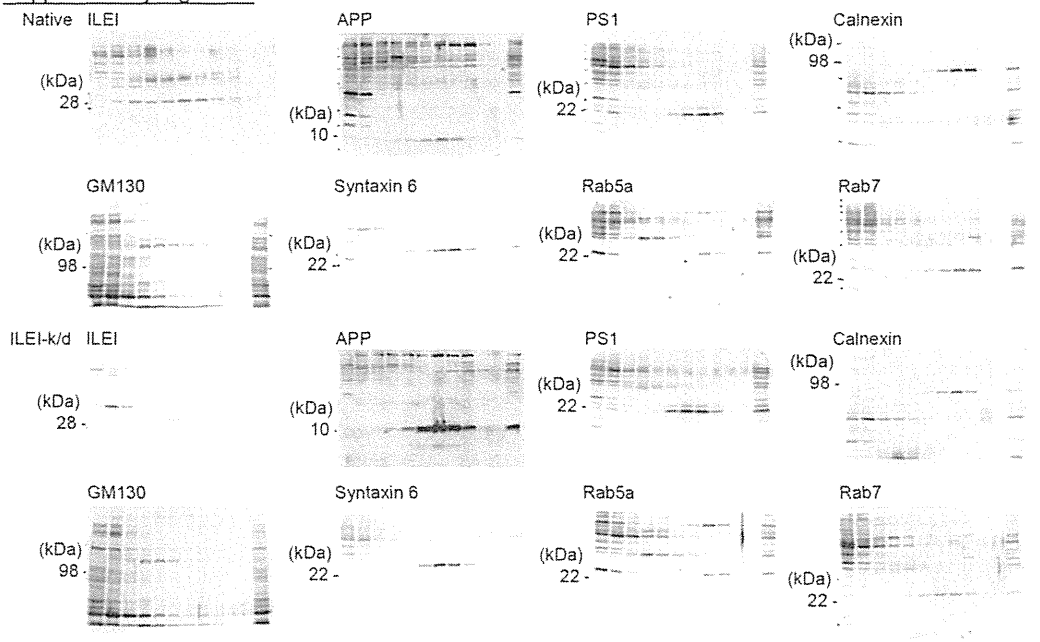

Supplementary Figure 10 continued.

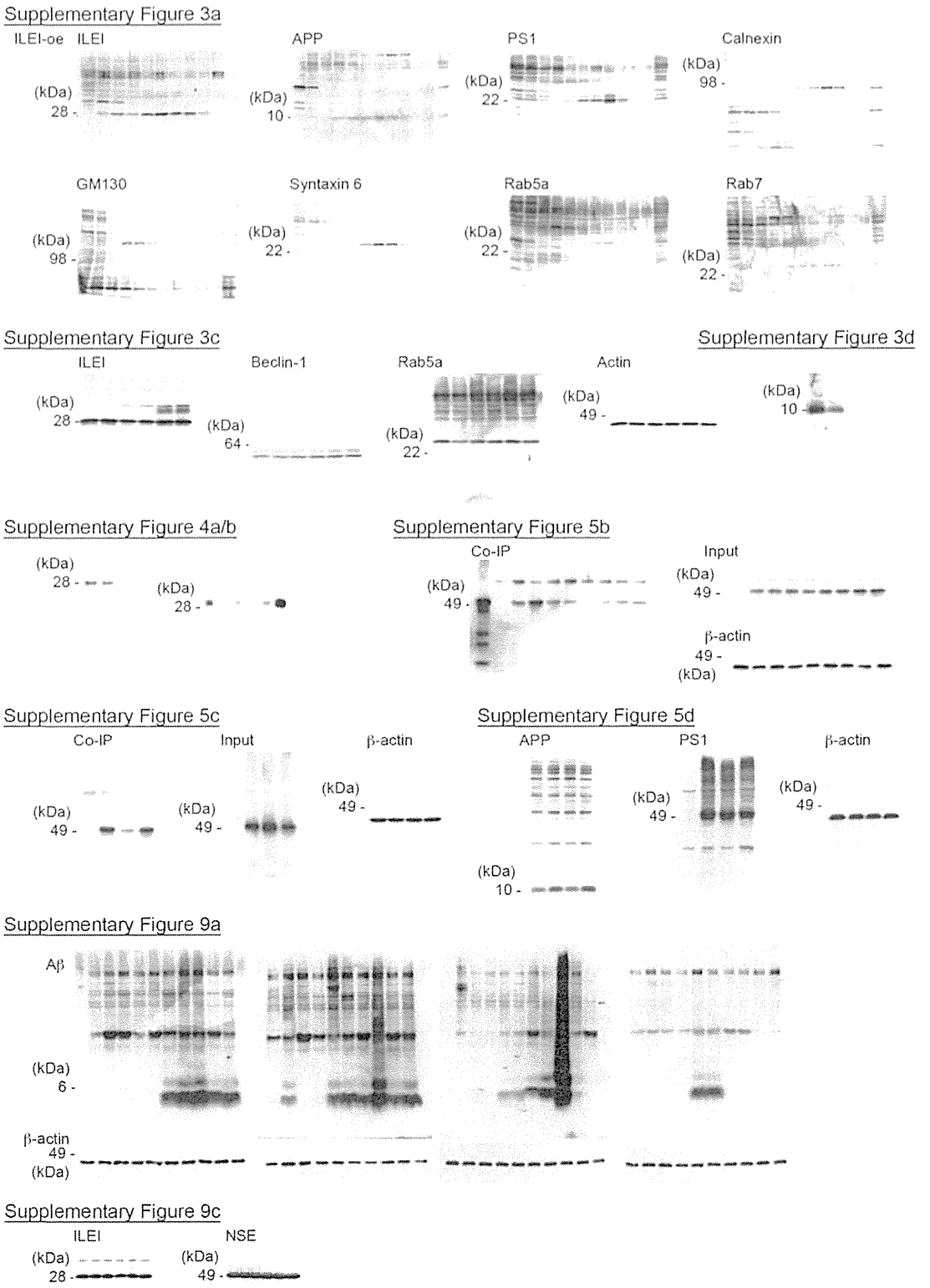

Supplementary Figure 10 continued.

Acta Neuropathol (2014) 127:303–305
DOI 10.1007/s00401-013-1191-9

CORRESPONDENCE

3R and 4R tau isoforms in paired helical filaments in Alzheimer's disease

Masato Hasegawa · Sayuri Watanabe · Hiromi Kondo · Haruhiko Akiyama · David M. A. Mann · Yuko Saito · Shigeo Murayama

Received: 20 August 2013 / Revised: 29 September 2013 / Accepted: 30 September 2013 / Published online: 9 November 2013

Isoform-specific tau antibodies RD3 and RD4 are useful tools for investigating expression and localization of three-repeat (3R) and four-repeat (4R) tau isoforms. Recently, transition from 3R to 4R tau in Alzheimer's disease (AD) was proposed based on immunohistochemical studies with RD3 and RD4 [3]. Here, we show that two factors influence immunoreactivity to these antibodies. First, deamidation at the RD4 epitope abrogates immunoreactivity to RD4, and second, presentation of RD3 and RD4 epitopes is reciprocally affected by protease. Asparagine at position 279 in the RD4 epitope is predominantly deamidated to aspartic acid in pathological tau in AD brains [2, 4]. Consequently, the presence of 4R tau in AD pathologies may be underestimated when RD4 is used. However, anti-4R (available from Cosmo Bio Co., Ltd.) raised against RD4 peptide with N279D substitution stained both wild-type and deamidated 4R tau, and strongly stained RD3+/RD4− tangles and smearing tau fragments in Sarkosyl-insoluble fraction of AD brain [2].

It was reported that RD3 stained abundant ghost tangles in entorhinal cortex and tangles in CA1, but failed to stain fine processes of tangles and threads [3], while RD4 failed to detect ghost tangles in entorhinal cortex [3]. To understand these findings, we examined the influence of protease on immunoreactivity. Paraffin sections of AD brains were treated with 10 μg/mL Proteinase K (Pro-K) for 30 min after autoclaving (Ac) and formic acid (FA) treatment. RD3 staining was strongly enhanced (Fig. 1a, b). Conversely, RD4 immunoreactivity almost completely disappeared after Pro-K treatment (Fig. 1c, d). Not only ghost tangles but also RD3−/RD4+ tangles and their processes became RD3-positive after Pro-K treatment (Fig. 1a, b), strongly suggesting that the RD3 epitope was buried in tau filaments of intracellular tangles and threads, and was exposed by Pro-K treatment. Contrary to expectation, anti-4R staining was also enhanced by Pro-K treatment (Fig. 1e, f). It is possible that the recognition site of anti-4R is distinct from that of RD4 and is exposed by Pro-K treatment of sections. Anti-4R antibody may recognize the carboxyl-half of the antigen peptide, while RD4 recognizes the amino-terminal half around N279. Pro-K treatment was also effective in immunostaining of free-floating AD sections with a lower concentration.

To confirm these findings biochemically, Sarkosyl-insoluble fractions from two AD brains were treated with trypsin or Pro-K, then immunoblotted with RD3, RD4, anti-4R and anti-pS396 (Fig. 1g–j). RD3 strongly stained many bands and smears, as seen with pS396 (Fig. 1g, j),

M. Hasegawa (✉) · S. Watanabe
Department of Neuropathology and Cell Biology, Tokyo Metropolitan Institute of Medical Science, Setagaya-ku, Tokyo 156-8506, Japan
e-mail: hasegawa-ms@igakuken.or.jp

H. Kondo
Histology Center, Tokyo Metropolitan Institute of Medical Science, Setagaya-ku, Tokyo 156-8506, Japan

H. Akiyama
Dementia Research Project, Tokyo Metropolitan Institute of Medical Science, Setagaya-ku, Tokyo 156-8506, Japan

D. M. A. Mann
Centre for Clinical and Cognitive Neuroscience, Institute of Brain Behavior and Mental Health, University of Manchester, Salford M6 8HD, UK

Y. Saito
Department of Laboratory Medicine, National Center Hospital, NCNP, 4-1-1 Ogawahigashi, Kodaira, Tokyo 187-8502, Japan

S. Murayama
Department of Neuropathology, Tokyo Metropolitan Institute of Gerontology, Itabashi-ku, Tokyo 173-0015, Japan

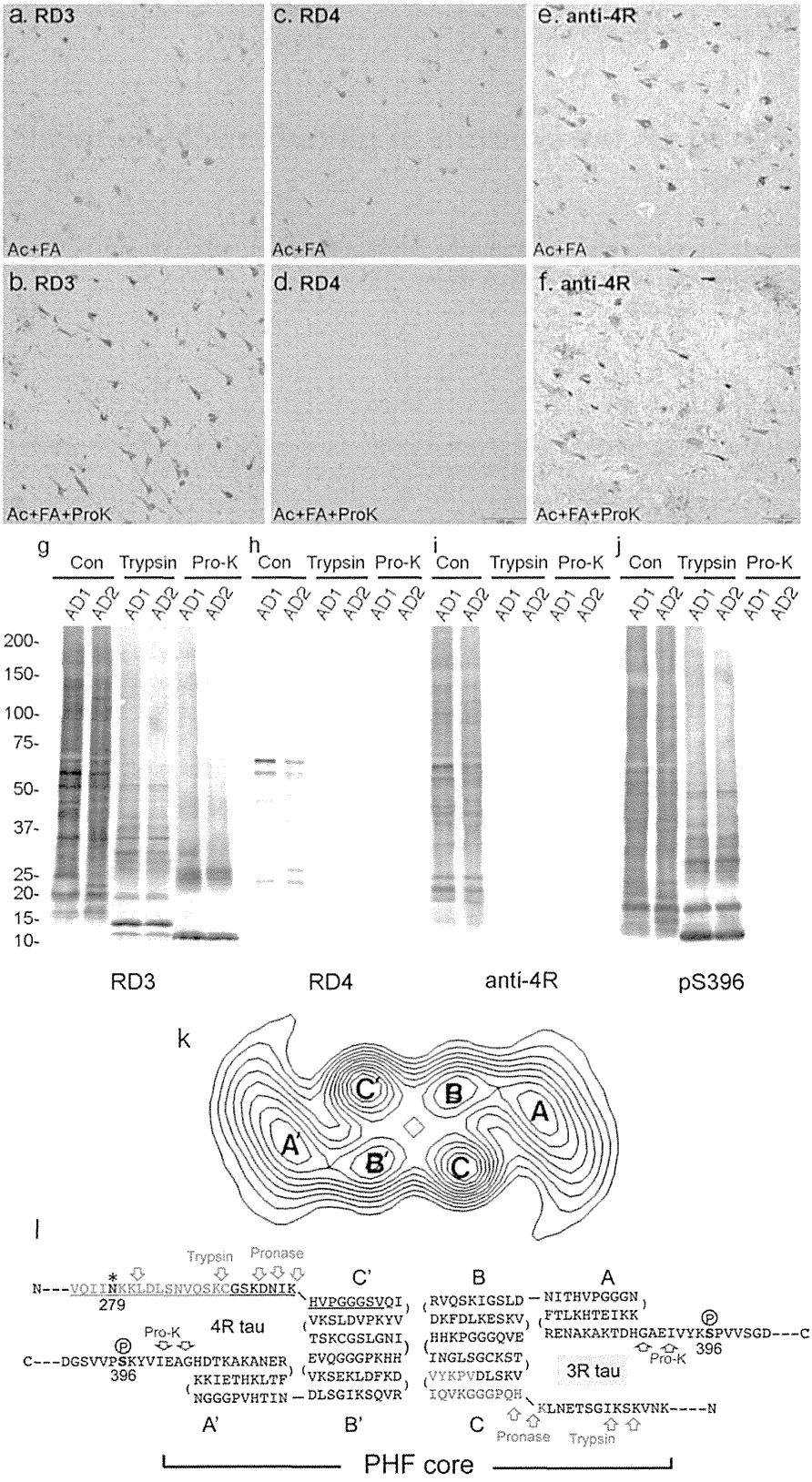

Fig. 1 **a–f** Immunostaining of AD sections after Ac and FA treatment before (**a**, **c**, **e**) and after (**b**, **d**, **f**) Pro-K treatment, using RD3 (**a**, **b**), RD4 (**c**, **d**) and anti-4R (**e**, **f**). *Bar* 100 μm. **g–j** Immunoblots of Sarkosyl-insoluble tau from two AD brains, before (*Con*) and after treatments with trypsin or Pro-K, using RD3 (**g**), RD4 (**h**), anti-4R (**i**) and pS396 (**j**). **k–l** Computed cross-section through a paired helical filament (**k**) [reproduced from Ref. [1], with permission of the publisher], a predicted folding model of 3R and 4R tau in PHF (**l**). RD3 and RD4 epitopes are indicated by *blue* and *red*, respectively. 4R tau specific insertion is indicated by *underlining*. The deamidation site N279 is indicated by *asterisks*. Phosphorylation of Ser396 is indicated. Possible trypsin, pronase and Pro-K cleavage sites are indicated in *green*, *purple* and *dark blue arrows*, respectively. The protease-resistant domain of PHF is indicated as *PHF-core*

whereas RD4 only labeled the 64/68 kDa doublet and some fragments at ~25 kDa (Fig. 1h). Anti-4R strongly stained the smears and fragments (Fig. 1i), suggesting that tau in these RD4-negative anti-4R-positive bands and smears is deamidated at N279. The weak RD4 and strong anti-4R immunoreactivities were completely abolished after trypsin or Pro-K treatment (Fig. 1h, i). This result is inconsistent with the immunohistochemistry, but protease sensitivity is likely different in fixed tissues. In contrast, the RD3 epitope was retained in the fragments, and RD3 strongly reacted with the protease-resistant 10–25 kDa bands after trypsin or Pro-K treatment (Fig. 1g). pS396 epitope was removed by Pro-K but not trypsin, suggesting a location outside the PHF core. Trypsin may not cleave the KSP site because of phosphorylation of Ser396. These results demonstrate reciprocal effects of protease treatment on RD3 and RD4 epitopes, indicating that RD4 epitope in tau in AD is susceptible to proteases, while RD3 epitope is highly resistant.

These results are consistent with previous findings. Wischik et al. identified two types of amino acid sequences, QPGGGKVQIVYK... (3R tau) and IKXVPGG... (4R tau), in 12-kDa tau fragment comprising the pronase-resistant core of PHFs [6] (see Fig. 1k). We identified HQPGGG... (3R tau) and HVPGGG... (4R tau) in 7–15 kDa trypsin-resistant fragments of PHF-tau in AD brains [5]. In both cases, 3R and 4R tau isoforms were detected, but the 4R tau N-terminus lacked the RD4 epitope. Based on these observations and a computed cross-section of PHF (Fig. 1k) [1], we propose a schematic model of tau folding in PHF (Fig. 1l). Analysis of the cross-sectional density in the PHF core on electron micrographs indicates the presence of two C-shaped morphological units, which correspond to the two strands of PHF, each with three domains (Fig. 1k) [1]. The RD3 epitope is buried in the PHF core and is normally masked by the N- or C-terminal region of tau, but is exposed in ghost tangles and/or in PHFs attacked by proteases. The RD4 epitope, which is mostly deamidated in PHF, is located slightly outside the core, where it can be digested by proteases (Fig. 1l). This model can explain the epitope masking of RD3 and RD4 and the reciprocal effects of degradation or protease treatment on the immunoreactivities.

This study indicates that differential presentation of epitopes can occur as a result of folding and processing, even when the epitopes are located in close proximity. Tau in PHFs appears to be processed gradually by intracellular proteases and more extensively in extracellular space during AD progression. We suggest that changes in immunoreactivity to antibodies reflect aging of tau in tangles or PHFs, which are composed of both 3R and 4R tau isoforms. We also show that Pro-K treatment of sections after Ac and FA treatment is useful for unmasking buried epitopes.

Acknowledgments We acknowledge the support of Alzheimer's Research UK and Alzheimer's Society through their funding of Manchester Brain Bank under the Brains for Dementia Research (BDR) initiative. This work was supported by Grants-in-Aid for Scientific Research (S) (JSPS KAKENHI 23228004), (A) (JSPS KAKENHI 23240050), and MHLW Grant 12946221 (to M.H.).

References

1. Crowther RA (1991) Straight and paired helical filaments in Alzheimer disease have a common structural unit. Proc Natl Acad Sci USA 88:2288–2292
2. Dan A, Takahashi M, Masuda-Suzukake M, Kametani F, Nonaka T, Kondo H, Akiyama H, Arai T, Mann DM, Saito Y, Hatsuta H, Murayama S, Hasegawa M (2013) Extensive deamidation at asparagine residue 279 accounts for weak immunoreactivity of tau with RD4 antibody in Alzheimer's disease brain. Acta Neuropathol Commun 1:54
3. Hara M, Hirokawa K, Kamei S, Uchihara T (2013) Isoform transition from four-repeat to three-repeat tau underlies dendrosomatic and regional progression of neurofibrillary pathology. Acta Neuropathol 125:565–579
4. Hasegawa M, Morishima-Kawashima M, Takio K, Suzuki M, Titani K, Ihara Y (1992) Protein sequence and mass spectrometric analyses of tau in the Alzheimer's disease brain. J Biol Chem 267:17047–17054
5. Hasegawa M, Watanabe A, Takio K, Suzuki M, Arai T, Titani K, Ihara Y (1993) Characterization of two distinct monoclonal antibodies to paired helical filaments: further evidence for fetal-type phosphorylation of the tau in paired helical filaments. J Neurochem 60:2068–2077
6. Wischik CM, Novak M, Thogersen HC, Edwards PC, Runswick MJ, Jakes R, Walker JE, Milstein C, Roth M, Klug A (1988) Isolation of a fragment of tau derived from the core of the paired helical filament of Alzheimer disease. Proc Natl Acad Sci USA 85:4506–4510

EJN EUROPEAN JOURNAL OF NEUROSCIENCE

FENS

European Journal of Neuroscience, Vol. 40, pp. 2701–2706, 2014 doi:10.1111/ejn.12633

DISORDERS OF THE NERVOUS SYSTEM

Regional analysis of striatal and cortical amyloid deposition in patients with Alzheimer's disease

Kenji Ishibashi,[1] Kiichi Ishiwata,[1] Jun Toyohara,[1] Shigeo Murayama[2] and Kenji Ishii[1]

[1]Research Team for Neuroimaging, Tokyo Metropolitan Institute of Gerontology, 35-2 Sakae-cho, Itabashi-ku, Tokyo 173-0015, Japan

[2]Department of Neurology, Tokyo Metropolitan Geriatric Hospital, 35-2 Sakae-cho, Itabashi-ku, Tokyo 173-0015, Japan

Keywords: ^{11}C-Pittsburgh Compound B, Alzheimer's disease, amyloid, positron emission tomography, striatum

Abstract

We aimed to analyse the detailed distribution pattern of amyloid-β (Aβ) in the striatum, and to examine whether there is any correlation between Aβ deposition levels in the striatum and cortical regions. Twenty patients with Alzheimer's disease underwent positron emission tomography using ^{11}C-Pittsburgh Compound B (^{11}C-PiB) to quantify the Aβ deposition. Volumes-of-interest analyses were performed on the ventral striatum (VST), pre-commissural dorsal caudate (pre-DCA), post-commissural caudate (post-CA), pre-commissural dorsal putamen (pre-DPU), and post-commissural putamen (post-PU), followed by exploratory voxel-wise analyses. Volumes-of-interest analyses of ^{11}C-PiB binding showed: VST > pre-DPU ($P = 0.004$), VST > pre-DCA ($P < 0.0001$), pre-DPU > post-PU ($P < 0.0001$), and pre-DCA > post-CA ($P < 0.0001$), consistent with visual inspection of the ^{11}C-PiB images. Exploratory voxel-wise analyses of ^{11}C-PiB binding showed a positive correlation between the VST and the medial part of the orbitofrontal area ($P < 0.01$ family-wise error corrected). This study confirmed that there were ventral > dorsal, and anterior > posterior gradients of Aβ deposition in patients with Alzheimer's disease, and provided the first evidence of a robust correlation between Aβ deposition levels in the VST and the medial part of the orbitofrontal area. There are well-known anatomical and functional links between these areas. These findings indicated that brain Aβ deposition was not randomly distributed, but had characteristic patterns related to anatomical connectivity and/or functional networks.

Introduction

The positron emission tomography (PET) radioligand, ^{11}C-Pittsburgh Compound B (^{11}C-PiB) has been shown to possess high affinity and high specificity for fibrillar amyloid-β (Aβ) (Mathis *et al.*, 2002; Klunk *et al.*, 2003; Lockhart *et al.*, 2005; Ye *et al.*, 2005; Rowe & Villemagne, 2013). Using ^{11}C-PiB and PET enables us to visualise and quantify the amount of Aβ deposition, which is a useful biomarker for the diagnosis of Alzheimer's disease (AD) (McKhann *et al.*, 2011; Sperling *et al.*, 2011). The main brain regions showing ^{11}C-PiB binding are the frontal and posterior cingulate/precuneus cortices and the striatum (Vallabhajosula, 2011), consistent with known patterns of Aβ deposition, as described in post-mortem studies (Braak & Braak, 1991, 1997). The correlations between ^{11}C-PiB binding across different regions, and region-matched post-mortem measures of fibrillar Aβ deposition levels have previously been confirmed (Bacskai *et al.*, 2007; Ikonomovic *et al.*, 2008).

The Aβ deposition begins well before the onset of cognitive decline (Sperling *et al.*, 2011; Villemagne *et al.*, 2013), and the earliest deposition appears to be in the frontal and cingulate/precuneus regions (Mintun *et al.*, 2006). Compared with the cortical regions, detection of Aβ deposits in the striatum occurs at a later stage in AD progression (Braak & Braak, 1991; Thal *et al.*, 2002; Mintun *et al.*, 2006; Beach *et al.*, 2012). Some authors have indicated that Aβ plaques in the striatum are largely restricted to individuals with clinically-documented dementia (Braak & Braak, 1990; Thal *et al.*, 2002), although others have found plaques in clinically non-demented individuals (Wolf *et al.*, 1999). Moreover, recent studies have shown that striatal Aβ plaques correlate with the presence of dementia in patients with Lewy body disease (Kalaitzakis *et al.*, 2008, 2011). These findings indicate that Aβ deposition and neural circuits in the striatum are important for the regulation of cognition. There are, however, neither *in vivo* nor post-mortem studies that address the distribution pattern of Aβ deposition in the striatum in detail.

Martinez *et al.* (2003) anatomically divided the striatum into five subregions: ventral striatum (VST), dorsal caudate rostral to the anterior commissure (AC) [pre-commissural dorsal caudate (pre-DCA)], dorsal putamen rostral to the AC [pre-commissural dorsal putamen (pre-DPU)], caudate caudal to the AC [post-commissural caudate (post-CA)], and putamen caudal to the AC [post-commissural putamen (post-PU)] (Mawlawi *et al.*, 2001; Martinez *et al.*, 2003). The VST includes the nucleus accumbens, ventral caudate rostral to the AC, and ventral putamen rostral to the AC. The post-CA and post-PU include the caudate and putamen from the plane of the AC to the plane through the most caudal part of these regions.

The first aim of this study was to analyse the distribution patterns of Aβ deposition among the striatal subregions in patients with AD,

Correspondence: Kenji Ishibashi, as above.
E-mail: ishibashi@pet.tmig.or.jp

Received 10 March 2014, revised 17 April 2014, accepted 25 April 2014

using ^{11}C-PiB and PET. There is a concept that the molecular pathology leading to Aβ aggregation progresses through specific anatomical connections and/or functional networks (Seeley *et al.*, 2009; Raj *et al.*, 2012). Therefore, the second aim was to examine whether there are correlations between ^{11}C-PiB binding in cortical regions and any of the striatal subregions, and to discuss the relationship between any two related regions in the light of anatomical and functional connectivity. The associations between cognitive measures and ^{11}C-PiB binding were also assessed.

Materials and methods

Research participants

The present study was performed retrospectively. The subjects comprised 20 patients [8 men and 12 women; age 50–83 years (mean age 67.6 years, SD 9.4)] and 14 age-matched control subjects [nine men and five women; age 52–84 years (mean age 64.6 years, SD 9.8)]. All patients had no family history of early-onset dementia, and were diagnosed with AD at or after the time of ^{11}C-PiB PET scanning on the basis of clinical criteria (American Psychiatric Association, 1994). Apolipoprotein E genotype was measured in 13 of 20 patients. Five, six and two patients presented the 3/3, 3/4 and 4/4 apolipoprotein E genotype, respectively. For each patient, the diagnosis of AD was supported by the findings from ^{18}F-fluorodeoxyglucose PET, which is used to estimate the cerebral metabolic rates of glucose utilisation. Briefly, all patients showed decreased ^{18}F-fluorodeoxyglucose uptake in the posterior cingulate, precuneus, and temporoparietal cortices, as a typical pattern of AD (Sperling *et al.*, 2011). All patients also underwent magnetic resonance imaging (MRI), and did not show any significant findings except for cortical atrophy, presumably due to AD. All control subjects were defined as healthy on the basis of their medical history, the results of their physical and neurological examinations, and the MRI findings.

All participants underwent ^{11}C-PiB PET scanning at Tokyo Metropolitan Institute of Gerontology for research purposes, during the period from December 2006 to January 2013. At the time of ^{11}C-PiB PET scanning, the Mini Mental State Examination (MMSE) scores of the patients were 14–30 (mean 22, SD 5). The diagnosis of AD in each patient with a relatively high MMSE score was confirmed by the clinical course after ^{11}C-PiB PET scanning. The Ethics Committee of the Tokyo Metropolitan Institute of Gerontology approved this study protocol, and written informed consent was obtained from all of the patients. The study conformed to the World Medical Association Declaration of Helsinki published on the website of the Journal of American Medical Association in 2013.

Positron emission tomography scanning

The radioligand, ^{11}C-PiB, was synthesised as described previously (Wilson *et al.*, 2004) with slight modifications. PET scanning was performed on a scanner (SET-2400W; Shimadzu, Kyoto, Japan) in three-dimensional mode. Images with 50 slices were obtained with a 2.054 × 2.054 × 3.125-mm^3 voxel size and a 128 × 128 matrix size. The transmission data were acquired using a rotating ^{68}Ga/^{68}Ge rod source for measured attenuation correction. Static emission data were acquired for 40–70 min after intravenous bolus injections of ^{11}C-PiB. The injection doses were 462 ± 102 MBq, and the specific activities were 56.7 ± 46.4 MBq/nmol at the time of injection (mean ± SD). Data were reconstructed after correction for decay, attenuation, and scatter.

Magnetic resonance imaging acquisition and volumes of interest

The MRI scanning was performed using a 1.5-Tesla Signa EXCITE HD scanner (GE, Milwaukee, WI, USA) in three-dimensional mode (3DSPGR; repetition time, 9.2 ms; echo time, 2.0 ms; matrix size, 256 × 256 × 124; voxel size, 0.94 × 0.94 × 1.3 mm), and was processed using the FMRIB Software Library (FSL; Oxford University, Oxford, UK).

Volumes of interest (VOIs) included the striatal subregions as target regions, with the cerebellum as a reference region. A whole-striatum VOI was created by combining the caudate, putamen, and nucleus accumbens VOIs, anatomically defined in native space using FSL FIRST. The whole striatum was divided into five anatomical VOIs (Fig. 1A, C, and D): the VST, pre-DCA, post-CA, pre-DPU, and post-PU, as described in the Introduction (Mawlawi *et al.*, 2001; Martinez *et al.*, 2003). A cerebellum VOI (Fig. 1B and D) was created by transforming a bilateral VOI, drawn manually on the cerebellar cortex in Montreal Neurological Institute (MNI) 152 space, to native space using FSL FNIRT.

Positron emission tomography image processing

The static PET images were co-registered to the corresponding structural MRI using FSL FLIRT. The VOIs placed on the MRI were moved onto the PET images, and VOI-based analyses were performed. Activity data within the anatomically defined VOIs (see above) were extracted from co-registered PET images. ^{11}C-PiB binding for each VOI was quantified, with the cerebellum used as a reference region (Lopresti *et al.*, 2005; Ikonomovic *et al.*, 2008). The ratio (activity in the target region:activity in the cerebellum) was described as the standardised uptake value ratio (SUVR).

Data analysis and statistical analysis

The VOI-based analyses were performed to test the difference in SUVR values between the two striatal subregions using the paired

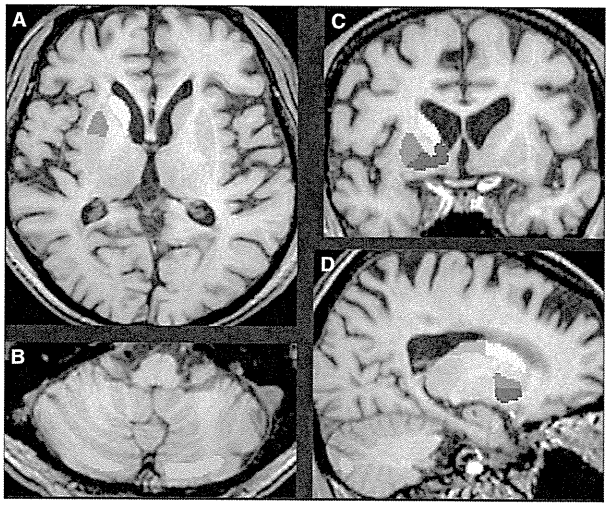

FIG. 1. An example of VOIs. VOIs placed on the VST (blue), pre-DCA (yellow), pre-DPU (red), post-CA (green), post-PU (light blue), and cerebellum (orange) are displayed in the axial (A and B), coronal (C) and sagittal (D) sections of a representative MRI image. One side of the VST, pre-DCA, pre-DPU, and post-CA VOIs, and both sides of the cerebellum VOI are shown.